



Leading Opinion

Bone as an inspiration for a novel class of mechanoactive materials[☆]Melissa L. Knothe Tate^{a,b,c,d,*}, Roland Steck^{a,d}, Eric J. Anderson^{a,b}^a Thinktank for Multiscale Computational Modeling of Biomedical and Bio-inspired Systems, Case Western Reserve University, Cleveland, OH, USA^b Department of Mechanical & Aerospace Engineering, Case Western Reserve University, Cleveland, OH 44106, USA^c Department of Biomedical Engineering, Case Western Reserve University, Cleveland, OH 44106, USA^d Orthopaedic Research Center, Cleveland Clinic, Cleveland, OH 44195, USA

ARTICLE INFO

Article history:

Received 22 May 2008

Accepted 15 September 2008

Available online 5 October 2008

Keywords:

Biomimetic material

Bone

Computational fluid dynamics

Elasticity

Finite element analysis

Mechanoactive material

Wound dressing

ABSTRACT

Fortuitous combinations of anisotropic stiffness and permeability coefficients in a poroelastic structure (e.g. bone) result in counterintuitive flow when the structure is subjected to tension or compression. Nonlinearities in flow and transport result when loading is asymmetrical (tension and compression are not balanced over the course of a cycle), boundary conditions are asymmetrical (area available for inflow or outflow) or uptake of the transported agent is factored in (ratchet effect). These properties can be exploited for the development of flow directing materials, e.g. wound dressings that prevent development of stress concentrators while augmenting transport of pharmaceuticals to the wound site, as well as transport of drainage away from the wound site, via convective flow. The dressings are designed as carriers of pharmaceutical agents. Normally, the delivery of these agents is diffusion driven, e.g. as in nicotine, pain abatement, and hormone replacement therapy patches. However, by designing the structure of the pharmaceutical doped dressings to mimic the relationship between stiffness and permeability coefficients shown to produce counterintuitive flow in bone, it is possible to deliver the pharmaceuticals to the wound site and imbibe exudant from the wound in an accelerated fashion via convective transport. This unprecedented approach harnesses the mass and movement of the patient to provide the impetus for flow to and from the wound. It has a range of further applications in not only the medical sector but also the textile industry as well as in microfluidics.

© 2008 Elsevier Ltd. All rights reserved.

1. Introduction

All life on Earth is water derived, and all living biological materials contain water. Cyclic loading due to weight bearing activities in Earth's gravitational environment as well as natural forces such as wind induce fluid to flow through biological materials, including live wood, tissue, and soil. Flowing fluid is the medium of life for cells inhabiting Earth's biomaterials. A major impasse in understanding fluid flow through biological materials is the difficulty in visualizing complex flow fields that result from physiologic or natural activity. During the past decade, great

emphasis has been placed on elucidation of load-induced flow through bone tissue, which serves as a model system for a relatively stiff yet porous two-phase material comprising 25% water (see Ref. [1] for a review of the subject).

The fluid and solid phases of bone exhibit anisotropy at multiple length and time scales. Modeling the interplay between the mechanical behavior and physiology of bone depends on the length and time scale of the physiological system of interest. For instance, the skeletal system exhibits a length scale with order of magnitude (O) of 10^{-1} m in the mature organism, takes approximately 18 years to manufacture and has an approximate design life upwards of 80 years (considering maximum mean life expectancy as a measure of design life [2]). The peak material performance of the skeleton lies somewhere between the 18th and 30th year of life (taking peak bone mass, as defined by the National Institute of Arthritis and Musculoskeletal and Skin Diseases, as a measure of material performance [3]). At the length scale of an articular joint such as the hip joint (O 10^{-2} m), its design life can be estimated as less than 70 years, given current statistics on hip replacement patients [4]; interestingly, hip replacement implants are given a nominal 15 year design life [5]. At the tissue scale (O 10^{-3} m) the interplay between the fluid and solid phases of bone is a critical determinant in bone

[☆] Editor's Note: This paper is one of a newly instituted series of scientific articles that provide evidence-based scientific opinions on topical and important issues in biomaterials science. They have some features of an invited editorial but are based on scientific facts, and some features of a review paper, without attempting to be comprehensive. These papers have been commissioned by the Editor-in-Chief and reviewed for factual, scientific content by referees.

* Corresponding author. Department of Mechanical & Aerospace Engineering, Case Western Reserve University, Glennan 418, 10900 Euclid Avenue, Cleveland, OH 44106, USA. Tel.: +1 216 368 5884; fax: +1 216 368 4969.

E-mail address: knothetate@case.edu (M.L. Knothe Tate).

physiology. Cells are the living constituents of bone tissue, and osteocytes embedded within mineralized spaces called lacunae depend for survival on convective flow for nutrient delivery and waste transport via vascular and extravascular fluid spaces [6]. Cell death is an indicator of pathophysiological processes which presage tissue, organ and system failure [7]. Whereas death and replenishment of cells in healthy bone is a stochastic process in balance, cell death outweighs replenishment in diseased bone [7]; hence, cell health influences tissue health and cell death affects the connectivity of the pericellular fluid network [7].

Molecular transport through the extravascular fluid channels and pores of the bone matrix is highly dependent on size, charge and conformation of a given molecule as well as mechanical loading which induces pressure gradients that displace fluid in bone tissue (Fig. 1). The heart provides the pressure gradient for flow of blood (itself a multiphase material comprising red blood cells and plasma) through vascular channels but the resistance to flow in the extravascular spaces is too high and the pressure gradient is likely too damped for efficient extravascular flow. The increased resistance to flow in extravascular space is due to the smaller prevailing length scale of these channels (smaller than cells as well as smaller than the fenestrae of blood vessels, $O 10^{-6}$ – 10^{-9} m). Mechanical loading due to physiological activity is a putative means for displacing fluid through the spaces linking vascular channels to cells; to differentiate it from the flow of blood through the vascular channels, it is referred to as extravascular flow, or pericellular flow within fluid spaces surrounding cells [1,6,8].

Recent work emphasizes the role of the cells in bone, in particular stem cells, in building bone during in utero development and throughout postnatal life (see Ref. [9] for a recent review). Cells build and inhabit bone throughout life. Entombed within the bone mineral, osteocytes live for up to 25 years. They are considered replenishable or immortal, as stem cells deriving from the periosteum (outer sheath) and the marrow (inside the bone) continue to divide and give rise to more cells over time. However, the so-called proliferation rates of cells decrease with age. Furthermore, for a given osteocyte within the cortex to be replaced, osteoclasts must

first excavate a channel through the bone to make space for new bone apposition by osteoblasts. Osteoblasts that become trapped in the matrix they are producing metamorphose into osteocytes [9]. At and below the length scale of the cell, the interplay between the mechanical and biological function is key for the transport characteristics of molecules including nutrients, growth factors, and waste products.

During in utero development, already before the first beating of the heart and contraction of the skeletal muscles, the stem cells deriving from the sperm and the egg are exposed to spatially and temporally varying biophysical and chemical signals that instruct the cells to become specialized, for example as a bone cell or a cartilage cell or a muscle cell. As such, musculoskeletal development in utero represents the *de novo* formation of a time dependent material by cells in response to mechanical and chemical signals. If a tissue engineer wants to mimic nature, she might apply stresses including dilatational and deviatoric stresses to the cells in a bioreactor or perfusion chamber, in the lab, to grow the tissue prior to implanting it in the body. The magnitude and duration of such stresses in utero are radically different than those to which mature, differentiated (specialized) cells are exposed to in the adult organism [9,10]. In contrast to the time (years) and length (macro) scale of adaptation of adult bone, the time scale of biological events in utero is relatively short (measured in days) and at the length scale of the cell; biologically relevant events may occur at even shorter time scales. For example, unspecialized mesenchymal stem cells adapt after only 1 h of exposure to shear stress via fluid drag. Exposure to shear stress results in a rapid up regulation in production of structural matrix proteins, such as collagen, that dampen the signal experienced by the cell. It also upregulates the production of cytoskeletal proteins that serve as the scaffolding or buttressing for the cell [11]. Hence, already after 1 h of exposure to stress, mesenchymal stem cells build a composite structure [11]. Taking into account longer periods of time, at longer length scales, tissue forms and its anisotropy reflects spatial and temporal effects of mechanical and chemical cues experienced by the cells within [9,10].

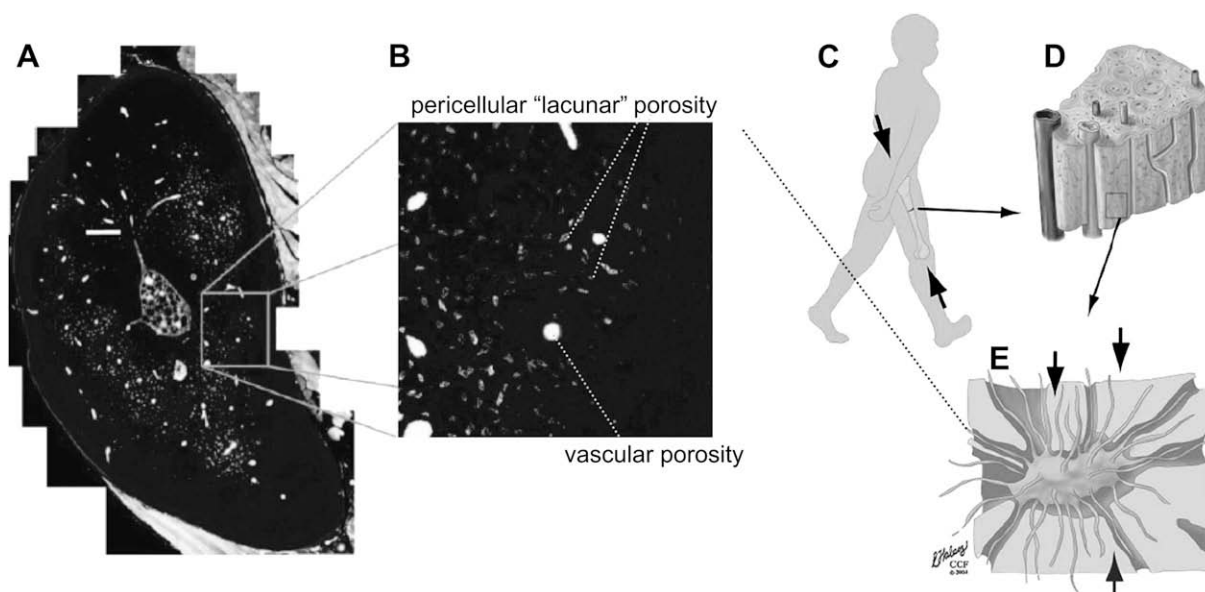


Fig. 1. Vascular and extravascular fluid transport in bone. A: an epifluorescent micrograph of the rat ulna in cross section. The scale bar (to the left, and above the central medullary canal) comprises approximately 1 mm. Light areas indicate presence of a fluorescent tracer that was administered via intravenous injection. In the center of the section, the large intramedullary canal contains bone marrow. Smaller vascular channels emanate from the medullary canal in the plane of the image and from the cortex, orthogonal to the plane of the image. B: vascular canals are an order of magnitude larger than pericellular spaces. C: weight bearing loads cause pressure gradients to build in the bone, resulting in displacement of fluid within extravascular spaces. D: at the tissue scale, vascular canals are visible. E: osteocytes are entombed in bone mineral and depend on fluid transport through the extravascular spaces for nutrients and waste disposal. C–E: after [35].

Once bone is formed, there are further mechanisms by which the cells can adapt the architecture of the composite to optimize structure for function. Typically, this involves osteoclastic resorption, where bone resorbing cells remove mineralized matrix to create space for bone building osteoblasts to lay down new material. This is much like patching a structure rather than tearing it down and building anew. The resulting structural properties reflect a balance of effects from taking away old bone and laying down new bone, which is highly dependent on time.

Several decades ago, it was postulated that under load, bone acts as a stiff, fluid filled sponge [12,13]. Hence, under compression, a pressure gradient forms, forcing fluid from the smaller pericellular spaces to the larger fluid spaces around vascular canals (like fluid exuding from a fluid filled sponge under compression). In contrast, reversal of that pressure gradient would result in fluid imbibement (like fluid imbibement under tension). A body of literature provides experimental support for load-induced fluid flow through poroelastic tissues such as bone and ligaments (see Ref. [14] for the first description of poroelasticity and Ref. [1] for a recent review of fluid flow in bone). However, a major impasse in understanding bone fluid flow effects at the cell and tissue level is the difficulty in visualizing complex flow fields that result from physiologic activity. Poroelastic finite element (FE) methods provide an elegant tool to predict load-induced fluid flow in virtual models of bone [15,16]; such FE based studies have provided valuable insight into physiological effects of fluid flow such as enhancement of nutrient and bioactive molecule transport via convective means [16].

The effective implementation of poroelastic finite element models of bone is limited by lack of experimentally measured material parameters such as permeability at the inner and outer surfaces of bone (endosteum and periosteum, respectively), which would be expected to exert great influence on the development and relaxation of pore pressure gradients within bone. Although the periosteal surface is often idealized as completely sealed or impermeable, it is known from experimental studies that the periosteum is well vascularized and that bone matrix apposing vascular spaces exhibits at least two degrees of porosity (matrix pores and pericellular pores). At the other extreme, the endosteal surface is often idealized as a freely permeable boundary. A further shortcoming of state-of-the-art models is the lack of site specific or spatially resolved material parameters, *i.e.* bone is typically idealized as a homogeneous material. However, recently published histological data indicate that the microstructure of bone tissue adapts to the predominant local loading mode to which bone is subjected and, thus, shows a high degree of spatial specificity [19,20]. Furthermore, in long bones, porosity increases from the periosteum to the endosteum due to higher remodeling rates in the vicinity of the endosteal as compared to the periosteal surface [21]. Hence, the lack of spatial resolution in definition of material parameters may negatively impact the accuracy of fluid flow predictions in virtual bone models. This is expected to be particularly true when comparing flow profiles through specific regions of bone, *e.g.* along the neutral axis as opposed to flow through regions under highest tensile and compressive loads. These limitations are further exacerbated by limitations inherent to commercially available software, such as finite element modeling programs, where the definition of nontrivial boundary conditions is cumbersome or impossible. Previous studies implemented very low stiffness “virtual” boundary layers [16,22,23] that allowed for the simulation of boundary permeabilities over a wide range without affecting the elastic behavior of the bone.

Computational models of flow through bone modeled as a perfect isotropic poroelastic material, *i.e.* as a continuum with porosity and permeability evenly distributed in space show an increase in mass transport due to convection versus diffusion alone.

The effect of the load-induced fluid flow on molecular transport within bone was found to be maximal in the middle of the cortex, especially in the lateral and the medial aspect of the bone cross section. When the concentration of the simulated tracer substance was averaged over the thickness of the cortex for different sectors of the cross section, the difference between the loaded and unloaded bone was bigger on the tension side than on the compression side. Furthermore, in accordance to the results of the experimental study, the concentration difference decreased with increasing loading frequency [16,22,24]. Experimental models corroborated these findings, but a high degree of site specificity was observed in tracer transport across the bone's cross section, indicating that the idealization of bone as a perfect, fluid filled sponge may not be appropriate [16,26,27]. Also, previous parametric studies underscored the importance of appropriate boundary conditions for accurate prediction of time dependent flow properties in bone [25–27].

Hence, the initial impetus of the current study was to predict the effect of site specific permeabilities at bone surfaces (boundary conditions) and within the bone cortex (site specific material properties) on fluid velocities and pore pressures, using a parametric study on an idealized cylindrical bone model. Thereafter, the goal was to measure site specific material parameters using high resolution images of bone samples and to implement these measured site specific properties to predict actual flow velocities and pressure distributions in rat ulnae. Finally, in the process of elucidating the effect of site specific material parameters on flow through bone, an apparent conundrum in flow through bone was deciphered and then exploited to develop a novel class of mechanoreactive materials.

2. Parametric study of spatially varying material properties, boundary conditions in bone

An idealized cylindrical bone model was implemented to study the effect of spatially varying material properties and boundary conditions on model predictions. To maximize comparison with experimental data obtained using a four-point-bending model of the rat tibia and an end loading model of the rat ulna [28], the computational model geometry was implemented at the length scale (30 mm length, 2.8 mm outer diameter and 1.4 mm inner diameter) of the rat ulna. A combined compressive (1.3 N) and bending (1.5 N) load was applied to mimic the physiological loading of most long bones, which would be equivalent to compressing the cylinder via axial compression concomitant to applying four-point-bending. For computational efficiency, we reduced the geometry and loading conditions further, exploiting the inherent symmetry of the cylinder in the sagittal plane (Figs. 2C and 3; both halves experience symmetric pore pressure and fluid velocity distributions) and the inherent symmetry of the combined load case at mid-length of the cylinder (Fig. 2C; mirroring the loading condition about the constrained in would result in combined four-point-bending and compression).

The cylindrical bone model was divided into concentric layers around the medullary canal (1.4 mm in diameter) to represent the anatomical layers of cortical bone, from inside to outside, including the endosteum, three layers of concentric cortical bone, and the outermost periosteum. Cortical bone was modeled as a transverse isotropic material with an 11.5 GPa modulus of elasticity in the transverse direction and 17 GPa in the longitudinal direction. The Poisson's ratio was defined as 0.58 in the transverse plane and 0.31 in other planes [16–18].

There are a paucity of quantitative data describing the magnitudes and spatial distributions of porosities and permeabilities in cortical bone (as shown in following section). In fluid filled porous materials such as soil and bone, porosity specifies

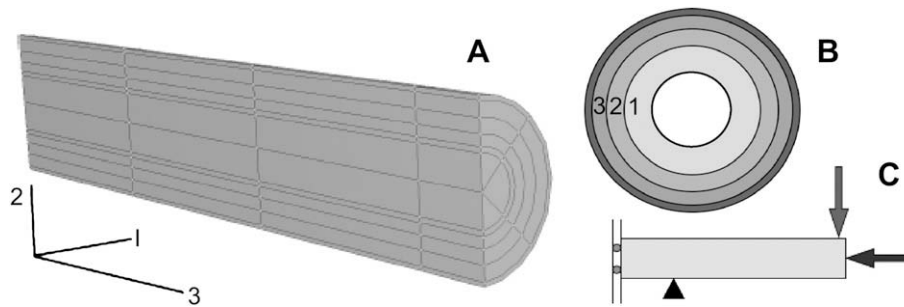


Fig. 2. Cylindrical bone model to study the effect of spatially varying material properties and boundary conditions on flow predictions. The bone is idealized as a cylinder (A, sectioned in half as depicted, along the sagittal plane of symmetry), loaded in combined compression and bending (C). Due to the symmetry of the load about the middle of the cylinder length, one half of the loading geometry is depicted (C); the full loading condition is inferred by mirroring about the mid-length plane (double lines in loading schematic). Material properties are defined for three concentric regions of the cortex (B).

the ratio of pore volume to the total volume of material. Permeability describes the capacity of the fluid to flow through the material and depends on pore connectivity as well as size. For example, an abundance of unconnected pores confers zero permeability (*i.e.* impermeable) to a porous material [29]. In contrast, for a porous material with non-zero connectivity between pores, permeability increases with increasing pore size (flow rate increases for a given pressure gradient) [29], as defined by Darcy's Law [30].

Since actual values vary depending on species, age, health status and bone of interest [6], a parametric approach lends itself to predict the influence of porosity and permeability on fluid velocity and pore pressure distribution in bone (see below for a more physical description of these variables). Four scenarios were studied to cover a broad spectrum of porosities and permeabilities and their relative spatial distribution (Table 1). Porosity (Φ) and permeability (k) were treated as co-dependent variables in these calculations, with a linear relationship for $^{10}\log(k) = f(\Phi)$. This assumption is frequently implemented in soil mechanics models,

and is the basis for the k - Φ plots used to estimate permeability from the porosity for a given texture type [31].

For the purposes of our model, the permeability in the radial direction, k_{11} , is assumed to be an order of magnitude higher than the permeability in the circumferential direction, k_{22} , and two orders of magnitude higher than the permeability in the longitudinal direction, k_{33} , since pericellular spaces around cell processes (canaliculi) are preferentially oriented in the radial direction (emanating radially outwards from the medullary canal with respect to the bone long axis and radially outwards from a given vascular canal with respect to the bone long axis) (Table 1). Of note, if we had accounted for vascular permeability, k_{33} would have exhibited the highest permeability, since vascular canals tend to be organized longitudinally in rat cortical bone. For each case modeled, porosity is assumed to increase with increasing proximity to the endosteum.

The two component force was applied to the model to create a combined compressive bending load of sinusoidally varying amplitude (1 Hz frequency), resulting in a longitudinal surface

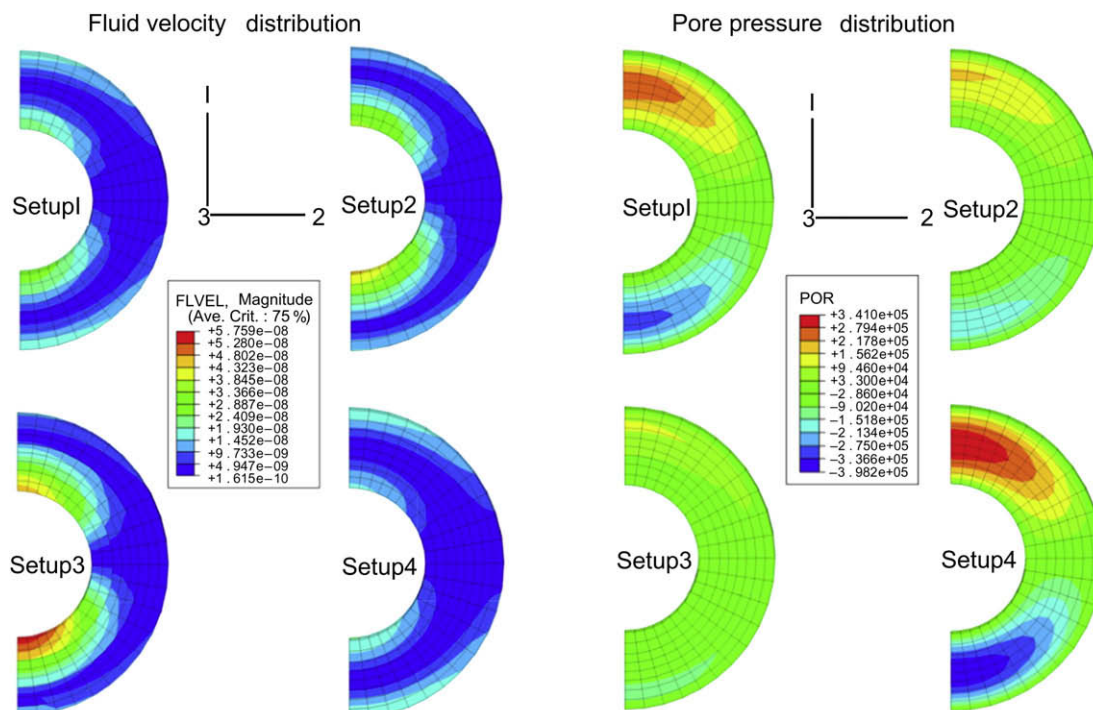


Fig. 3. Fluid velocities and pore pressures were predicted for each parameter set. The spatial distribution of velocities and pore pressures was highly dependent on material parameter definitions. Half of the cylinder cross section is depicted due to symmetry about the sagittal plane (see Fig. 2A).

Table 1
Porosity and permeability values used in parametric study

Parameter set	Cortex region	Porosity (%)	Porosity $\Delta_{\max-\min}$	Void ratio	Permeability		
					k_{11}	k_{22}	k_{33}
Setup 1	1	7	2	0.075	2.47E-20	2.47E-21	2.47E-22
	2	6		0.064	1.58E-20	1.58E-21	1.58E-22
	3	5		0.053	1.00E-20	1.00E-21	1.00E-22
Setup 2	1	10	5	0.111	1.00E-19	1.00E-20	1.00E-21
	2	8		0.087	3.71E-20	3.71E-21	3.71E-22
	3	5		0.053	1.00E-20	1.00E-21	1.00E-22
Setup 3	1	15	10	0.176	1.00E-18	1.00E-19	1.00E-20
	2	10		0.111	1.00E-19	1.00E-20	1.00E-21
	3	5		0.053	1.00E-20	1.00E-21	1.00E-22
Setup 4	1	5	0	0.053	1.00E-20	1.00E-21	1.00E-22
	2	5		0.053	1.00E-20	1.00E-21	1.00E-22
	3	5		0.053	1.00E-20	1.00E-21	1.00E-22

Porosity (%) is the *per cent* of the total volume comprising pores or voids. In contrast, the void ratio is defined as the ratio of pore or void volume to total volume, i.e. porosity/1 – porosity [29].

strain of 1000 microstrain, which mimics physiological loading. Fluid velocities and pore pressures were calculated in the poroelastic cylindrical model using the finite element program Abaqus (Simulia, Providence, Rhode Island). The model consisted of 2146 hexahedral elements in total; the cortical bone was made up from 3 radial elements, 8 elements along the half-circumference, and 37 elements along the length of the model. The previously described four parameter sets were implemented for each model to determine the relative influence of site specific porosities and permeabilities on pore pressure and load-induced fluid velocities. The resulting fluid velocity and pore pressure predictions were plotted for a cross section at the middle of the cylinder (Fig. 3). The distribution of fluid velocity and pore pressure in the model bone cross section was highly dependent on the definition of properties including porosity and permeability. In general, decreasing porosity resulted in increasing pore pressure within the bone cortex. In both the radial and circumferential directions, flow velocity increases with increasing porosity. The relative changes in flow velocity and pore pressures remain on the same order of magnitude for porosities ranging from 5 to 15%. Although the overall pore fluid pressure distribution calculated with this poroelastic shell layer model was comparable to the pressure distribution determined in a previous model with uniform material parameters [16], the spatial distribution of fluid velocity and pore pressure varied significantly (Fig. 3). This study confirmed the importance of site specific material parameters in the prediction of interstitial fluid flow in mechanically loaded bone, providing the impetus to measure spatial distribution of porosity in rat ulnae.

3. Measurement of spatially resolved porosities and permeabilities

To determine the spatial distribution of porosity in two dimensions, a collage of high resolution confocal micrographs was produced by imaging the rat ulna in cross section (Fig. 4D). The

binary image of individual fields of view (Fig. 4A) was segmented, using image analysis algorithms, to differentiate between pericellular (Fig. 4B) and vascular (Fig. 4C) porosity. The respective porosity distributions were then replotted for the whole cross section to produce spatial “heat maps” of each respective porosity (high porosity concentration depicted as warm red colors, low concentration depicted as cool blue colors, Fig. 4E, F).

These plots demonstrate that osteocyte density varies strongly with increasing distance from the medullary cavity. In the vicinity of the endosteum, the bone is highly organized and consolidated, exhibiting fewer osteocytes than the mid-cortex, where the bone is less organized and more cellular. The degree of organization/consolidation increases again towards the periosteum with concomitant decrease in osteocyte density. Furthermore, vascular density and therefore vascular porosity varies with distance from the endosteum as well. Of particular interest, areas with the highest density of pericellular spaces do not necessarily co-localize with areas showing the highest density of vascular spaces.

Thus the modeling of the cortex as a series of concentric shells with distinct porosity and permeability parameters appears appropriate for the rat ulna. The two orders of magnitude of bone porosity exhibit distinct and independent spatial patterns. Using k - Φ plots, permeabilities can be calculated for the respective measured porosities. Hence, the distinct and independent distribution of pericellular and vascular porosity in space will yield highly anisotropic permeability parameters for bone tissue. Alternatively, the measured vascular porosity can be used to define the elastic properties of cortical bone at different sites within the cross section, as porosity has been shown to be inversely and exponentially related to bone strength and modulus [19,20]. Recent studies demonstrate a novel method to measure actual pericellular network permeabilities using scaled up physical models of actual cellular networks in healthy, human cortical bone. Using this method, permeabilities on the order of $2.8 \times 10^{-16} \text{ m}^2$ were measured for the network devoid of cells; virtual inclusion of cellular structures in post hoc numerical models reduces the permeability of the pericellular network to the order of 10^{-17} – 10^{-18} m^2 [30]. Previous estimates reported a permeability of $1.47 \times 10^{-20} \text{ m}^2$ for the pericellular (lacunocanalicular) fluid space, based on theoretical models designed to elucidate electromechanical behavior observed in bone bending experiments [32].

4. The condundrum: role of anisotropy in counter-intuitive flow

By modeling bone as a poroelastic hollow cylinder, we elucidated the relative roles of anisotropic permeabilities and stiffnesses on flow through bone. Under a combined compressive and bending load, pore pressures and resulting fluid velocities were calculated as a function of spatially varying porosity and stiffness. In general, pore pressure provides the impetus for the fluid to flow and the fluid moves in the direction of least resistance to flow. Hence, for a given pressure gradient, flow velocities increase with increasing porosity. For decreasing porosities, higher pressures are required to move the fluid. Interestingly, in these parametric models, we observed negative pore pressures within the cylindrical sections subjected to compressive loading, and positive pore pressures within sections subjected to tensile loading. We reported similar observations previously [27,33], where some regions of compression were associated with areas of negative pore pressure (hence imbibing fluid) and some regions of tension were associated with areas of positive pore pressure (hence exuding fluid). Based on the current parameter study, this counterintuitive flow can be attributed to the effective expansion of the flow volume in the radial direction during compression and the effective compression of the volume in the radial direction during tension. Combined with

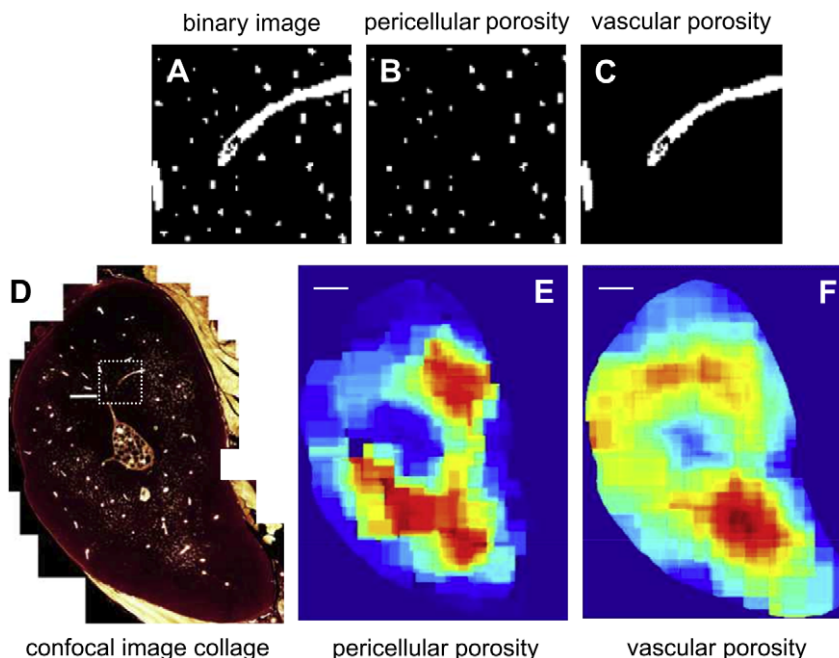


Fig. 4. Spatial distribution of pericellular and vascular porosities are visualized in high resolution confocal micrographs of the rat ulna, stained to highlight all fluid spaces in the bone. D: multiple high resolution micrographs are obtained and collaged to view the qualitative distribution of pores in the cross section. Individual images (A) are segmented to distinguish the small caliber pericellular porosity (B) from the vascular porosity (C). Density plots are created by mapping regions with highest (warmest colors) and lowest (coolest colors) numbers of pores per area. Regions depicted in A–C are magnified from dashed white box in D. Scale bars in D–F: 1 mm.

fortuitous stiffness, porosity and/or permeability parameters, squeezing of the stiff, fluid filled bone “sponge” results in imbibement of fluid while exerting tensile loads on the sponge results in exudation of fluid. This can also be envisioned as a type of buckling behavior for the anisotropic bone section, where areas under tension expand radially, resulting in efflux of fluid orthogonal to the plane, and areas under compression shorten radially, resulting in influx of fluid orthogonal to the plane (Fig. 5).

5. Exploitation of permeability, porosity for flow directing materials

Having elucidated the effects of site specific material properties including permeability, porosity and/or stiffness in cortical bone, we then set out to exploit these properties to develop a novel class of mechanoactive materials that harness mechanical loads to direct flow within the material (Fig. 6) [34]. The flow directing materials technology can be applied in a variety of arenas. For instance, the technology lends itself well for mechanoactive wound dressings that prevent development of stress concentrators while augmenting transport of pharmaceuticals to the wound site, as well as transport of drainage away from the wound site, via convective flow. Such mechanoactive dressings can be designed as carriers of pharmaceutical agents. Normally, the delivery of pharmaceutical agents is diffusion driven, e.g. as in nicotine, pain abatement, and hormone replacement therapy patches. However, by designing the structure of the pharmaceutical doped dressings to mimic the relationship between stiffness and permeability coefficients shown to produce counterintuitive flow in bone, it is possible to deliver the pharmaceuticals to the wound site in an accelerated fashion via convective transport (Fig. 6). This novel approach harnesses the mass and movement of the patient to provide the impetus for flow to and from the wound.

The mechanoactive material technology is being developed with a scalable (from nm to cm), modular architecture in which an individual modules can be designed and manufactured in specific

patterns and at specific scales for the appropriate time domain and desired function. Feasibility of this concept has been shown *in silico* and *in vitro* in mechanistic experiments designed to show the spatial and temporal specificity of the technology. The goal of the first reduction to practice is to develop and prototype a compression module or unit patch that delivers drugs through “delivery dots” and imbibes fluid through the material surrounding the dots (Fig. 6A). The materials within and surrounding the delivery dots will exhibit defined permeability and stiffness properties that result in contrasting flow characteristics under mechanical loads such as tension and compression.

In silico models demonstrate that, depending on the definition of these material properties, the volume within and the volume surrounding the delivery dots exudes and imbibes fluid, respectively, under compression; this effect persists, with dampening, over ten time steps (e.g. seconds, Fig. 6B). In addition, parametric studies show that the direction and rate of drug delivery (Fig. 6C, dot exudation and surrounding imbibement, magnitude is plotted on a color scale and flow direction is shown by vector plots) and/or moisture wicking (Fig. 6D, dot imbibement and surrounding exudation, magnitude plotted as color, direction as vector) can be controlled precisely through the choice of these material parameters. In contrast, if homogeneous material properties are employed, the patch fails to exhibit contrasting flows under compressive/tensile loading. In this case, uniform and ‘intuitive’ flow is controlled by the level of porosity and loading mode. Thus, through specific combinations of stiffness and permeability, concomitant drug delivery and moisture wicking be achieved using this approach. In addition, dual drug delivery can be achieved by design of dual exuding structures with convection parameters tuned for optimal pharmacokinetics of each respective drug. In sum, not only is the concept feasible, but also it can be exploited for a variety of functions.

Feasibility of this concept has been shown *in silico* and *in vitro* in mechanistic experiments designed to show the spatial and temporal specificity of the technology. The proposed approach to

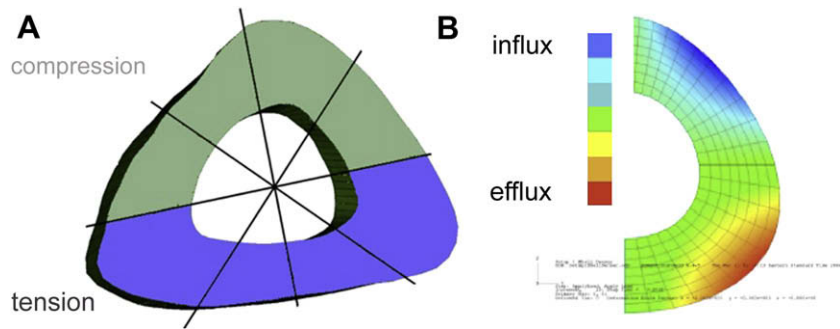


Fig. 5. Schematic of rat tibia cross section (A) and prediction of radial displacements resulting in fluid influx and efflux (B).

route flow through wound care dressings by harnessing the mechanical forces incurred through physical activity is unprecedented. If reduced to practice the proposed may lead to a new class of biomaterials. The development of this novel class of biomaterials can also potentially open up new paradigms for bio-agent delivery and/or clinical subterfuge of pathological processes, each of which represent new paradigms for enhancing human health and treating

diseases that endanger human health. A review of current and past medical literature revealed no previous reports of approaches similar to the proposed concept. A review of the patent record revealed prior art centered around two categories including foam wound dressings and drug delivery foams (US05891463, US6486378, US05462743, US06787682, US05939339); however, no prior art was observed for the class of wound dressings envisioned

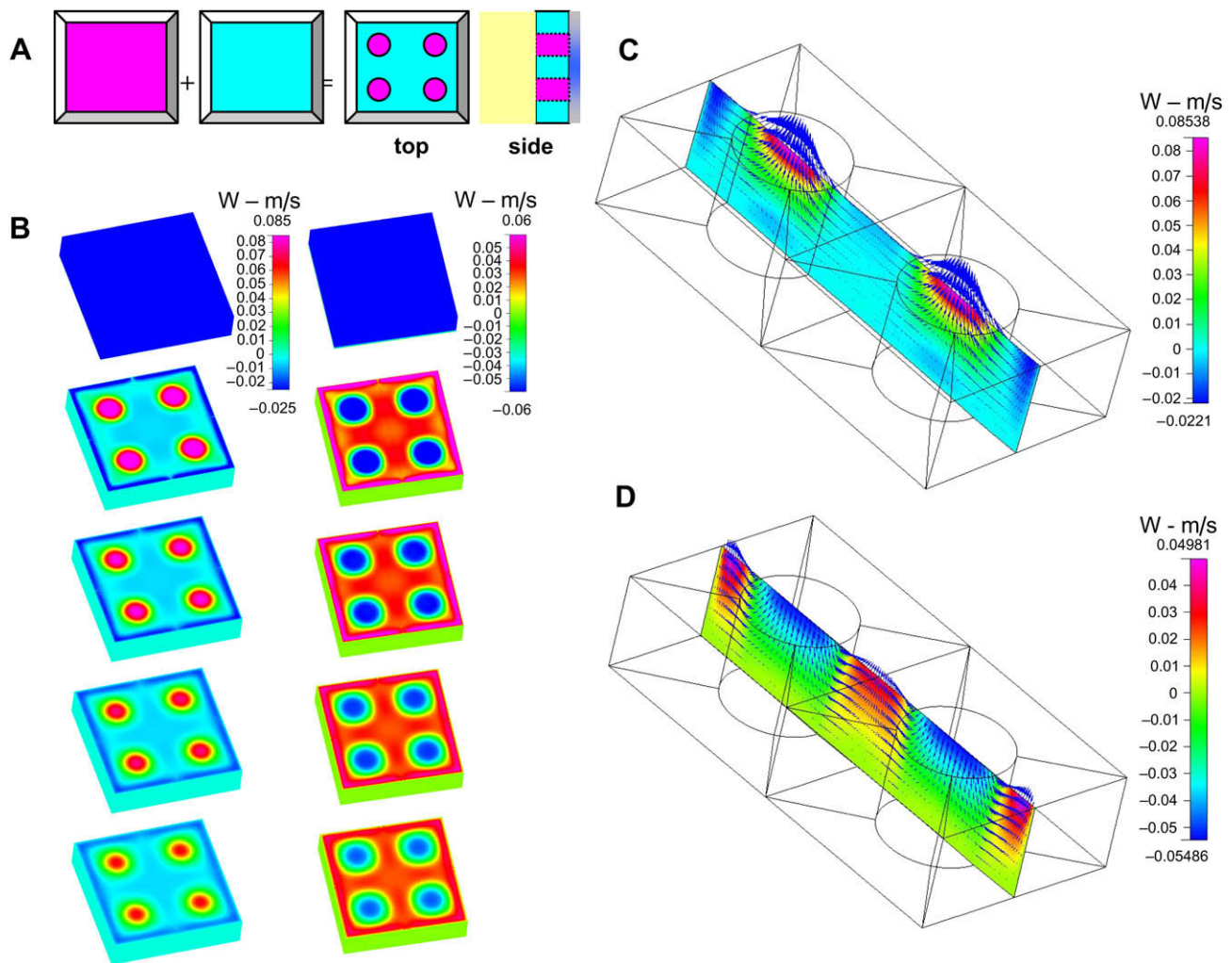


Fig. 6. Flow directing material design concept and *in silico* pilot studies. A. The novel class of flow directing materials: concept and feasibility testing. One unit of a composite material "patch", designed such that certain regions imbibe fluid under compression (pink) and other regions exude fluid under compression (green). An outer lining (gradient blue-grey) is a high slip material that minimizes friction and serves as a constraining boundary. B–D. Proof of concept based on computational fluid dynamics models showing mechanism of action with time lapse, t_{1-10} (B) and control of flow direction (exuding, C, and imbibing, D) through definition of regional stiffness and permeability. Baseline control (not shown) has homogeneous material properties and exhibits no directional flow properties beyond exudation under compressive and imbibement under tensile loads.

in the proposed research and development program, which places it as a disruptive technology in the wound care sector.

6. Conclusions and applications

Hence, anisotropy in bone tissue material properties influences the local and global flow regimes through compact bone. In previous studies using highly idealized models of bone as a poroelastic material, application of compression to certain areas of bone results in an *influx* of fluid to the area, rather than an *efflux* as would be expected (e.g. when compressing a sponge, fluid is squeeze *out* of the sponge). In the current study it could be shown that fortuitous combinations of anisotropic stiffness, porosity and/or permeability coefficients in a poroelastic structure result in counterintuitive flow when the structure is subjected to tension or compression. Nonlinearities in flow and transport result when loading is asymmetrical (tension and compression are not balanced over the course of a cycle), boundary conditions are asymmetrical (area available for inflow or outflow) or uptake of the transported agent is factored in (ratchet effect). We are applying this knowledge to develop a novel class of bioactive materials, e.g. for mechanoactive wound dressings that harnesses the mass and movement of the patient to provide the impetus for flow to and from the wound. The technology will be developed with a scalable (from nm to cm), modular architecture in which an individual module can be designed and manufactured in specific patterns and at specific scales for the appropriate time domain and clinical function. The technology has a range of further applications in not only the medical sector but also the textile industry as well as in microfluidics.

Acknowledgements

We would like to acknowledge the contributions of Hans Jörg Sidler, a student at the Swiss Federal Institute of Technology in Zurich, and Asvin Ganapathi, a student at Stanford University, for their contribution to the modeling studies described in this manuscript.

This work was supported in part by funding from the Swiss National Science Foundation, National Science Foundation ADVANCE grant (Academic Career in Engineering and Science, i.e. ACES) program, Ohio Board of Regents sponsored Clinical Tissue Engineering Center, and the Coulter Case Translational Research Partnership. Part of this investigation was conducted in a facility constructed with support from Research Facilities Improvement Program Grant Number C06 RR12463-01 from the National Center for Research Resources, National Institutes of Health.

Conflict of interest

The authors confirm that there are no known conflicts of interest associated with this publication and that there has been no significant financial support for this work that could have influenced its outcome.

References

- [1] Knothe Tate ML. "Whither flows the fluid in bone?" An osteocyte's perspective. *J Biomech* 2003;36:1409–24.
- [2] Mathers CD, Loncar D. Projections of global mortality and burden of disease from 2002 to 2030. *PLoS Med* 2006;3:2011–30.
- [3] National Institute of Arthritis and Musculoskeletal and Skin Diseases, National Institutes of Health, Department of Health and Human Services. Osteoporosis: peak bone mass in women. Available from: http://www.niams.nih.gov/Health_Info/Bone/Osteoporosis/bone_mass.asp; March 2005.
- [4] Merrill C, Elixhauser A. Hospital stays involving musculoskeletal procedures, 1997–2005. Healthcare Cost and Utilization Project, Statistical Brief #34. Rockville, MD: Agency for Healthcare Research and Quality. Available from: <http://www.hcup-us.ahrq.gov/reports/statbriefs/sb34.pdf>; July 2007.
- [5] Murray DW, Carr AJ, Bulstrode C. Survival analysis of joint replacements. *J Bone Joint Surg Br* 1993;75:697–704.
- [6] Knothe Tate ML, Niederer P, Knothe U. In vivo tracer transport through the lacunocanalicular system of rat bone in an environment devoid of mechanical loading. *Bone* 1998;22:107–17.
- [7] Knothe Tate ML, Adamson JR, Tami AE, Bauer TW. The osteocyte. *Int J Biochem Cell Biol* 2004;36:1–8.
- [8] Anderson EJ, Knothe Tate ML. Open access to novel dual flow chamber technology for *in vitro* cell mechanotransduction, toxicity and pharmacokinetic studies. *Biomed Eng Online* 2007;6:1–6. Available from: <http://www.biomedical-engineeringonline.com/content/6/1/46>; 2007;6.
- [9] Knothe Tate ML, Falls TD, McBride SH, Atit R, Knothe UR. Mechanical modulation of osteochondroprogenitor cell fate. *Int J Biochem Cell Biol* 2008;40:2720–38.
- [10] McBride SH, Knothe Tate ML. Modulation of stem cell shape and fate A: the role of density and seeding protocol on nucleus shape and gene expression. *Tissue Eng Part A* 2008;14:1561–72.
- [11] McBride SH, Falls TD, Knothe Tate ML. Modulation of stem cell shape and fate B: mechanical modulation of cell shape and gene expression. *Tissue Eng Part A* 2008;14:1573–80.
- [12] Bassett CA. Electrical effects in bone. *Sci Am* 1965;213:18–25.
- [13] Piekarski K, Munro M. Transport mechanism operating between blood supply and osteocytes in long bones. *Nature* 1977;269:80–2.
- [14] Biot MA. General theory of three-dimensional consolidation. *J Appl Phys* 1941;12:155–64.
- [15] Manfredini P, Cocchetti G, Maier G, Redaelli A, Montevocchi F. Poroelastic finite element analysis of a bone specimen under cyclic loading. *J Biomech* 1999;32:135–44.
- [16] Steck R, Niederer P, Knothe Tate ML. A finite element analysis for the prediction of load-induced fluid flow and mechanochemical transduction in bone. *J Theor Biol* 2003;220:249–59.
- [17] Reilly DT, Burstein AH. The elastic and ultimate properties of compact bone tissue. *J Biomech* 1975;8:393–405.
- [18] Akhter MP, Raab DM, Turner CH, Kimmel DB, Recker RR. Characterization of in vivo strain in the rat tibia during external application of a four-point-bending load. *J Biomech* 1992;25:1241–6.
- [19] Riggs C, Lanyon LE, Boyde A. Functional associations between collagen fibre orientation and locomotor strain direction in cortical bone of the equine radius. *Anat Embryol (Berl)* 1993;187:239–48.
- [20] Sevostianov I, Kachanov M. Impact of the porous microstructure on the overall elastic properties of the osteonal cortical bone. *J Biomech* 2000;33:881–8.
- [21] Turner CH, Burr DB. Experimental techniques for bone mechanics. In: Cowin SC, editor. *Bone mechanics handbook*. 2nd ed. New York: CRC Press; 2001. p. 1–35.
- [22] Steck R, Niederer P, Knothe Tate ML. A finite difference model of load-induced fluid displacements within bone under mechanical loading. *Med Eng Phys* 2000;22:117–25.
- [23] Knothe Tate ML, Niederer P. A theoretical FE-based model developed to predict the relative contribution of convective and diffusive transport mechanisms for the maintenance of local equilibria within cortical bone. In: Clegg S, editor. *Advances in heat and mass transfer in biotechnology*. The American Society of Mechanical Engineers; 1998. p. 133–42. HTD – Vol. 362/BED – Vol. 40.
- [24] Knothe Tate ML, Steck R, Forwood MR, Niederer P. *In vivo* demonstration of load-induced fluid flow in the rat tibia and its potential implications for processes associated with functional adaptation. *J Exp Biol* 2000;203:2737–45.
- [25] Sidler HW, Steck R, Knothe Tate ML. Site-specific porosity and its impact on load-induced fluid movement in cortical bone. In: ASME summer bioengineering conference; 22–26 June 2005, Vail, CO. p. I-55.
- [26] Sidler H, Steck R, Knothe Tate ML. Site-specific porosity and its impact on load-induced fluid movement in cortical bone. In: Transactions of the 52nd annual meeting of the Orthopaedic Research Society, vol. 31; 2006. p. 1591.
- [27] Ganapathi AM, Steck R, Kaliyamoorthy S, Knothe Tate ML. A method for the implementation of appropriate boundary conditions in poroelastic bone models. In: Transactions of the 50th annual meeting of the Orthopaedic Research Society, vol. 29; 2004. p. 511.
- [28] Tami AE, Nasser P, Schaffler MB, Knothe Tate ML. Non-invasive fatigue fracture model of the rat ulna. *J Orthop Res* 2003;21:1018–24.
- [29] Lambe TW, Whitman RV. *Soil mechanics*. New York: John Wiley and Sons; 1969. p. 29.
- [30] Anderson EJ, Kreuzer SM, Small O, Knothe Tate ML. Pairing computational and scaled physical models to determine permeability as a measure of cellular communication in micro- and nano-scale pericellular spaces. *Microfluid Nanofluid* 2008;4:193–204.
- [31] Helle HB, Bhatt A, Ursin B. Porosity and permeability prediction from wireline logs using artificial neural networks: a North Sea case study. *Geophys Prospect* 2001;49:431–44.
- [32] Cowin SC. Bone poroelasticity. *J Biomech* 1999;32:217–38.
- [33] Steck R, Niederer P, Knothe Tate ML. Fluid flows through anisotropic, poroelastic bone models in the opposite direction to that through analogous isotropic models. In: ASME summer bioengineering conference; 25–29 June 2003, Key Biscayne, Florida. p. 213–4.
- [34] Knothe Tate ML, Anderson EJ. Flow directing materials and systems. US Patent No. 12106748; 2008.
- [35] Knothe Tate ML. Multi-scale computational engineering of bones: state of the art insights for the future. In: Bronner F, Farach-Carson C, Mikos A, editors. *Engineering of functional skeletal tissues*. London: Springer-Verlag; 2007. p. 141–60.